

LAMINAR-TO-TURBULENT TRANSITION OF YIELD-STRESS FLUIDS IN PIPE AND CHANNEL FLOWS

Shivam Prajapati^{1,2,*}, Prasoon Suchandra^{1,2}, Vivek Kumar^{1,2}, Ardalan Javadi¹, Suhas Jain¹, Cyrus Aidun^{1,2}

¹George W. Woodruff School of Mechanical Engineering, Georgia Institute of Technology, Atlanta, GA 30332, USA

²Renewable Bioproducts Institute, Georgia Institute of Technology, Atlanta, GA 30332, USA

ABSTRACT

We present direct numerical simulations (DNS) of laminar to turbulent transition in Herschel–Bulkley (HB) yield-stress fluids flowing through pipes and rectangular channels. The simulations employ a Herschel–Bulkley formulation that captures the yield-stress-driven plug, its breakdown, and the emergence of near-wall turbulent structures, enabling direct resolution of the transition mechanisms.

The DNS cover a broad range of generalized Reynolds numbers, $Re_G = 378$ to 5300, allowing us to resolve plug formation, transition onset, and fully turbulent regimes. In pipe flow, the simulations reproduce the characteristic transition sequence, which includes a strong plug and negligible turbulence at low Re_G , a sharp rise in turbulence intensity and u'_{rms} within a narrow transitional window ($Re_G \approx 2000$ to 3000), and wall-dominated turbulence with a weakened core at higher Re_G . Transition occurs only when local Reynolds stresses exceed the yield stress. The resulting regime boundaries ($Re_G < 1735$ laminar, $1735 < Re_G < 2920$ transitional, and $Re_G > 2920$ turbulent) align with trends reported for Carbopol fluids.

DNS of channel flow are performed in a 0.2 m streamwise domain using a $128 \times 129 \times 128$ grid (approximately 4.2 million cells). The simulations capture the same HB transition physics, including formation of a central plug, growth of near-wall turbulence observed via Q -criterion structures, and progressive strengthening of u'_{rms} and turbulent kinetic energy peaks with increasing Re_G . DNS also highlights the strong influence of shear-thinning and yield stress on transitional behavior.

This work provides the first DNS resolving the complete laminar to turbulent transition in HB fluids for both pipe and channel configurations, offering unified insight into plug breakdown, turbulence localization, and the role of yield stress in transition mechanisms. Experimental validation using a 3.6 m acrylic channel with particle image velocimetry (PIV) is planned to further assess the DNS predictions and quantify geometry-dependent

transition thresholds.

Keywords: Herschel–Bulkley fluid, laminar–turbulent transition, direct numerical simulation, yield-stress

NOMENCLATURE

Roman letters

u	velocity [m s^{-1}]
p	pressure [Pa]
u_τ	friction velocity [m s^{-1}]

Greek letters

ρ	density [kg m^{-3}]
τ_y	yield stress [Pa]
κ	consistency index [Pa s^n]
n	power-law index [-]

Dimensionless / statistics

Re_G	generalized Reynolds number [-]
Re_τ	friction Reynolds number [-]
u'_{rms}	r.m.s. velocity fluctuation [m s^{-1}]
I	turbulence intensity [%]

1. INTRODUCTION

Non-Newtonian complex liquids are important in applications ranging from red blood cell separation to interfacial phenomena in spray paints [1–4]. Quantifying these particles or bubbles are very critical [5, 6]. In future heat pipes research, shear-thinning behavior could reduce interfacial shear, thereby enhancing refrigerant transport [7, 8]. Yield-stress and shear-thinning fluids arise in a wide range of engineering and geophysical flows, including consumer products (e.g., Carbopol- and polymer-based formulations), slurry transport, and complex industrial processing. In fact, in pump design for pumping these kinds of high-viscosity liquids or slurry/bubbly flow [9, 10]. A central feature of Herschel–Bulkley (HB) materials is the coexistence of yielded and weakly-yielded (or unyielded) regions, which can produce plug-like cores and strongly non-uniform shear distributions. These rheological effects directly influence momentum transport and the onset and organization of turbulence in

*Corresponding author: sprajapati31@gatech.edu

Documentation for asmeconf.cls: Version 1.43, March 13, 2026.

wall-bounded configurations [11, 12]. Herschel–Bulkley rheology is also relevant in slurry transport, where the carrier fluid may exhibit both yield stress and shear-thinning behavior. These properties can lead to a plug-like core and a highly sheared wall region, which in turn affect the flow structure and pressure losses in pipes. This has been noted in studies of bentonite-based slurries, where the Herschel–Bulkley model provides a better description than simpler viscoplastic models when the shear-thinning response becomes important. For this reason, understanding transition in Herschel–Bulkley pipe and channel flows is also useful as a first step toward more realistic slurry-flow modeling [13, 14].

For Newtonian pipe flow, transition is classically mediated by localized structures such as puffs and slugs, and the associated intermittency has been documented extensively [12, 15, 16]. When the viscosity becomes shear-dependent, and especially when a finite yield stress is present, the transition scenario can change substantially: the flow may exhibit strong spatial intermittency, long-lived coherent structures, and pronounced asymmetry in the cross-section even under nominally symmetric forcing [17–20]. Experiments on yield-stress and shear-thinning pipe flows have reported robust transitional dynamics, including intermittent turbulent episodes and geometry-dependent asymmetry, across a range of rheologies and operating conditions [21–23]. Related transitions have also been explored in other non-Newtonian settings such as fiber suspensions and yield power-law flows in annuli, emphasizing the broader relevance of plug-dominated laminar states and their breakdown [24, 25].

On the modeling side, Reynolds-number scaling and transition correlations for non-Newtonian pipe flows have a long history, beginning with early generalized correlations and continuing through modern analyses and datasets [11, 26]. For the turbulent regime, DNS and high-fidelity simulations of shear-thinning pipe flows have clarified how shear-dependent viscosity modifies near-wall dynamics and turbulence statistics [27, 28]. In channel flow, canonical Newtonian DNS benchmarks remain a primary reference point for turbulence statistics and spectral content [12, 29], while recent studies have started to address generalized-Newtonian and yield-stress effects in turbulent channels [30]. However, despite these advances, a unified DNS picture that resolves the complete laminar–transitional–turbulent sequence in HB fluids including plug formation, plug breakdown, and the emergence of wall turbulence and that does so consistently across both pipe and planar/rectangular channel geometries remains limited.

The objective of the present work is to perform direct numerical simulations of HB yield-stress fluids in pressure-driven pipe and rectangular channel configurations over a broad range of generalized Reynolds numbers. We focus on resolving the transition dynamics and the accompanying changes in near-wall and core-region behavior, with particular attention to plug-dominated states and their evolution. For the pipe, we validate key transition metrics against experimental trends reported for Carbopol flows [20]. For the channel, we use a fully resolved three-dimensional domain and analyze statistical and spectral measures following common wall-bounded turbulence [12, 29, 31].

2. METHODOLOGY

2.1. Rheology model

We model the working fluid as a Herschel–Bulkley (HB) material characterized by yield stress τ_y , consistency index k , and power-law index n . In simple shear, the HB constitutive relation is

$$\tau = \tau_y + k\dot{\gamma}^n, \quad \text{for } \tau > \tau_y, \quad (1)$$

and the material remains unyielded when the applied stress is below the yield stress, so that $\dot{\gamma} = 0$ in that regime [30]. Setting $\tau_y = 0$ recovers the power-law model, while ($n = 1, \tau_y = 0$) gives the Newtonian limit.

For three-dimensional incompressible generalized-Newtonian simulations, we write the viscous stress tensor in terms of the strain-rate tensor S_{ij} as

$$\tau_{ij} = 2\nu(\dot{\gamma}) S_{ij}, \quad (2)$$

where $\nu = \mu/\rho$ is the kinematic viscosity. The effective strain rate is defined from the second invariant of S_{ij} as

$$\dot{\gamma} = \sqrt{2S_{kl}S_{kl}}. \quad (3)$$

For an HB fluid, the apparent kinematic viscosity is written as

$$\nu(\dot{\gamma}) = \frac{1}{\rho} \left(\frac{\tau_y}{\dot{\gamma}} + k\dot{\gamma}^{n-1} \right). \quad (4)$$

These expressions follow the standard generalized-Newtonian HB formulation used in prior DNS studies [11, 30].

Equation (4) becomes numerically stiff at very small $\dot{\gamma}$, and directly resolving an ideal yielded/unyielded split is challenging. We therefore use a bi-viscosity regularization in which the viscosity is capped below a cut-off strain rate $\dot{\gamma}_0$:

$$\nu(\dot{\gamma}) = \min \left(\nu_0, \frac{1}{\rho} \left(\frac{\tau_y}{\dot{\gamma}} + k\dot{\gamma}^{n-1} \right) \right), \quad (5)$$

with

$$\nu_0 = \frac{1}{\rho} \left(\frac{\tau_y}{\dot{\gamma}_0} + k\dot{\gamma}_0^{n-1} \right). \quad (6)$$

The cut-off $\dot{\gamma}_0$ is chosen small enough that it primarily affects nearly unyielded zones, while the yielded-region statistics remain unchanged within the accuracy of the simulations [11, 30].

2.2. Non-Newtonian Reynolds number

For HB fluids there is no single universally accepted Reynolds number because the viscosity varies with shear rate and the yield stress can produce unyielded regions [11]. Two conventions are particularly common in the literature. The first is the Metzner–Reed (MR) approach, originally introduced to extend Newtonian friction-factor correlations to non-Newtonian fluids [26]. The second is to define a generalized Reynolds number using a wall-viscosity scale, which is often convenient for wall-bounded transition and turbulence [27, 28, 30].

2.2.1. Generalized Reynolds number based on wall viscosity. we define the generalized Reynolds number as

$$Re_G = \frac{\rho UL}{\mu_w}, \quad (7)$$

where U is the bulk velocity and L is a characteristic length scale (pipe diameter D for pipe flow, and channel half-height h for channel flow). For HB fluids, the mean wall dynamic viscosity can be expressed in terms of the mean wall shear stress τ_w as

$$\mu_w = k^{1/n} \frac{\tau_w}{(\tau_w - \tau_y)^{1/n}}. \quad (8)$$

For a planar channel driven by a constant mean pressure gradient, $\tau_w = -h dP/dx$, while for a pipe τ_w can be obtained from the imposed pressure gradient in the conventional way [11, 30]. While engineering approaches such as the Chilton–Stainsby framework are useful for transport and pressure-loss estimation, the present study is aimed at resolving the physics of laminar-to-turbulent transition in Herschel–Bulkley flows through DNS, rather than developing a new correlation for design purposes.

2.2.2. Metzner–Reed Reynolds number. The Metzner–Reed idea is widely used for shear-dependent fluids and is commonly reported in turbulent pipe-flow studies of shear-thinning fluids [26–28]. For power-law fluids, a frequently used closed form is

$$Re_{MR} = \frac{8\rho U^{2-n} D^n}{k \left(6 + \frac{2}{n}\right)^n}, \quad (9)$$

which reduces to the Newtonian Reynolds number when $n = 1$.

For HB fluids, using a power-law Re_{MR} without explicitly accounting for τ_y does not collapse the laminar friction-factor relation across different yield-stress conditions. For this reason, a yield-stress-corrected Metzner–Reed Reynolds number for steady laminar planar channel flow can be written as [30]

$$Re_{MR,HB} = \frac{\rho U h}{\mu_w} \left(\frac{1+2n}{3n} \right) \left(\frac{1}{1 - a\chi - b\chi^2} \right), \quad (10)$$

where

$$a = \frac{1}{n+1}, \quad b = \frac{n}{n+1}, \quad \chi = \frac{\tau_y}{\tau_w}. \quad (11)$$

This construction ensures that the laminar friction relation collapses in a consistent way for HB channel flows [30]. We therefore report both Re_G and MR-based Reynolds numbers to enable direct comparison with the range of conventions used in experiments and DNS [11, 18, 20].

2.2.3. Friction Reynolds number. For inner scaling and near-wall normalization, we also use a friction Reynolds number based on the same wall-viscosity scale,

$$Re_\tau = \frac{\rho u_\tau h}{\mu_w}, \quad u_\tau = \sqrt{\frac{\tau_w}{\rho}}, \quad (12)$$

2.3. Governing equations

We solve the incompressible momentum equation in a form that is convenient for shear-dependent viscosity. For notational simplicity, the pressure, stress, and forcing are written in kinematic form (divided by the constant density), while we continue to refer to them as pressure, stress, and body force. Following this convention, the governing equation is

$$\frac{\partial \mathbf{u}}{\partial t} + \mathbf{u} \cdot \nabla \mathbf{u} = -\nabla p + \nabla \cdot \boldsymbol{\tau} + \mathbf{g}, \quad (13)$$

The stress tensor is modeled using the generalized-Newtonian (GN) assumption,

$$\boldsymbol{\tau} = 2\nu(\dot{\gamma}) \mathbf{s}, \quad (14)$$

where \mathbf{s} is the instantaneous strain-rate tensor (defined in Section 3.1) and $\nu(\dot{\gamma})$ is the apparent kinematic viscosity. In the present work, $\nu(\dot{\gamma})$ is obtained from the regularized Herschel–Bulkley model described in Section 3.1, rather than a power-law model. [28, 30]

For numerical robustness, the nonlinear term is implemented in a skew-symmetric form, so that the discrete system has improved stability properties. The implemented momentum equation is

$$\frac{\partial \mathbf{u}}{\partial t} + \frac{1}{2} (\mathbf{u} \cdot \nabla \mathbf{u} + \nabla \cdot (\mathbf{u}\mathbf{u})) = -\nabla p + \nabla \cdot (2\nu\mathbf{s}) + \mathbf{g}. \quad (15)$$

The forcing \mathbf{g} acts only in the streamwise direction and is set to achieve the desired bulk flow rate, while allowing the pressure field to remain periodic. [28]

When the time integration scheme benefits from treating a constant-viscosity Laplacian implicitly, the viscosity can be split into a spatially uniform reference value ν_{ref} plus a variable remainder. This yields

$$\frac{\partial \mathbf{u}}{\partial t} + \frac{1}{2} (\mathbf{u} \cdot \nabla \mathbf{u} + \nabla \cdot (\mathbf{u}\mathbf{u})) = -\nabla p + \nu_{\text{ref}} \nabla^2 \mathbf{u} + 2\nabla \cdot \{(\nu - \nu_{\text{ref}}) \mathbf{s}\} + \mathbf{g}. \quad (16)$$

In this form, the term $\nu_{\text{ref}} \nabla^2 \mathbf{u}$ can be advanced implicitly, while the remaining viscosity-dependent contribution is handled explicitly together with the other nonlinear terms, enabling stable time steps close to the CFL limit. [28]

3. DOMAIN DISCRETIZATION

3.1. Computational domains and mesh

3.1.1. Pipe flow. The pipe domain has a circular cross-section with radius $R = 25.4$ mm (diameter $D = 2R$) and a streamwise length $L = 4\pi D$, as illustrated in Fig. 1. The simulations use a structured O-grid topology generated with OpenFOAM’s bLockMesh. The O-grid provides smooth cell transitions and avoids excessively skewed cells near the wall. The radial spacing is clustered toward the wall using a geometric progression to better resolve the near-wall gradients and the interface between yielded and weakly sheared regions. The resulting mesh contains approximately 4×10^6 control volumes.

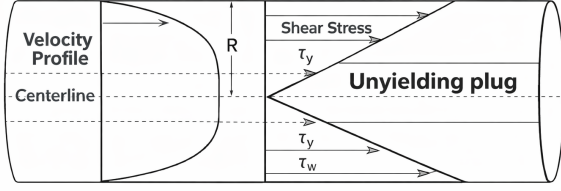


FIGURE 1: Pipe flow geometry and coordinate system.

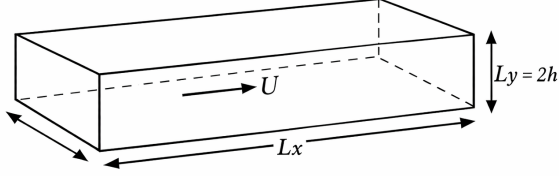


FIGURE 2: Channel flow geometry and coordinate system.

3.1.2. Channel flow. The channel domain is a rectangular box with streamwise length $L_x = 0.2$ m, as shown in Fig. 2. The streamwise, wall-normal, and spanwise directions are denoted by x , y , and z , respectively, with total channel height $L_y = 2h$. The channel simulations use a structured mesh of $128 \times 129 \times 128$ points in (x, y, z) , corresponding to approximately 4.2×10^6 cells.

A mesh-independence assessment was used to select the final grid. For both pipe and channel cases, the near-wall resolution satisfies $y^+ < 1$ based on the friction velocity and the first-cell center location.

4. RESULTS & DISCUSSION

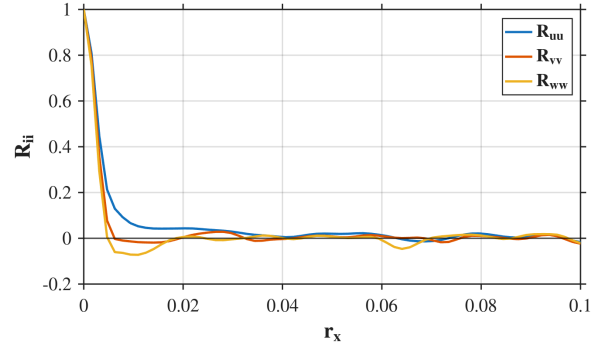
4.1. Domain-size sufficiency via two-point correlations.

For a periodic domain, domain-size sufficiency is assessed by verifying that the two-point correlations of velocity fluctuations converge to near zero at large separations in the periodic directions, indicating that the dominant structures are well contained within the computational domain. Two-point correlations of velocity fluctuations provide a direct and commonly used diagnostic for this purpose [12, 29]. In the channel, we therefore compute correlations in the streamwise direction at two representative wall-normal locations: a near-wall position and a position near the channel center. This is important because near-wall motions and outer-layer motions can exhibit different coherence lengths and characteristic spacings [12].

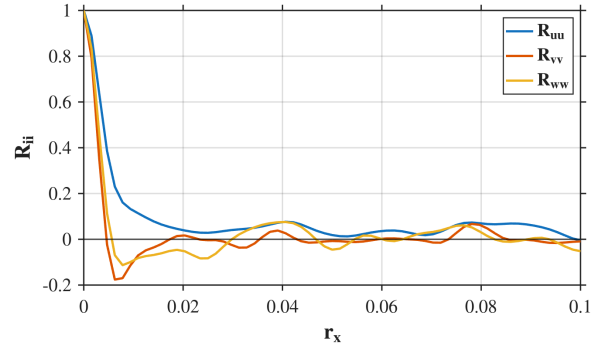
For the channel, where x is streamwise, y is wall-normal, and z is spanwise, we define the streamwise two-point correlations of the velocity fluctuations as

$$R_{ii}(r_x; y) = \frac{\langle u'_i(x, y, z, t) u'_i(x + r_x, y, z, t) \rangle_{z,t}}{\langle u_i'^2(x, y, z, t) \rangle_{z,t}}, \quad i \in \{u, v, w\}, \quad (17)$$

where $u'_i = \{u', v', w'\}$ are the fluctuating velocity components obtained after subtracting the time-averaged mean, and $\langle \cdot \rangle$ denotes averaging over the directions and time indicated by the subscripts. By construction, $R_{ii}(0; y) = 1$. The decay of R_{ii} with separation provides a quantitative measure of the coherence



(a) Near-wall location.



(b) Near-center location.

FIGURE 3: Streamwise two-point correlations in the channel for the velocity components u , v , and w : $R_{uu}(r_x; y)$, $R_{vv}(r_x; y)$, and $R_{ww}(r_x; y)$.

length of the corresponding velocity component and a practical check for periodic-domain sufficiency [12, 29]. Figure 3 shows the streamwise correlations $R_{uu}(r_x; y)$, $R_{vv}(r_x; y)$, and $R_{ww}(r_x; y)$ at the near-wall location (Fig. 3a) and near the channel center (Fig. 3b).

4.2. One-dimensional energy spectra

One-dimensional energy spectra are computed as a standard DNS diagnostic to quantify how turbulent kinetic energy is distributed across length scales in the homogeneous directions and to assess whether the selected grid resolution and domain size provide an adequate representation of the resolved range [29]. For the channel, we evaluate spectra in the streamwise direction.

Let $u'_i(\mathbf{x}, t) = u_i(\mathbf{x}, t) - \overline{u_i}(y)$ denote the fluctuating velocity component, where the overbar denotes averaging over time and the homogeneous directions at fixed wall-normal coordinate y . For a fixed y , we compute a Fourier transform in the streamwise direction,

$$\widehat{u}'_i(k_x, y, z, t) = \int_0^{L_x} u'_i(x, y, z, t) e^{-ik_x x} dx, \quad (18)$$

and form the one-dimensional streamwise energy spectrum of component i by averaging in time and integrating over the spanwise wavenumber,

$$E_{ii}(k_x, y) = \left\langle \int |\widehat{u}'_i(k_x, k_z, y, t)|^2 dk_z \right\rangle_t. \quad (19)$$

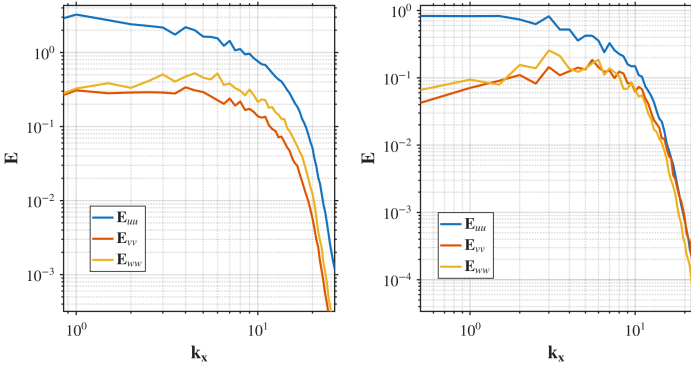


FIGURE 4: One-dimensional streamwise energy spectra in the channel at a near-wall location and at the channel center: $E_{uu}(k_x)$, $E_{vv}(k_x)$, and $E_{ww}(k_x)$.

TABLE 1: Flow conditions and Herschel–Bulkley parameters for 0.1% Carbopol pipe flow, adapted from Guzel et al. [20].

U (m/s)	$\dot{\gamma}$ (s^{-1})	τ_y (Pa)	k ($Pa \cdot s^n$)	n	Re_G
1.20760	1–220	1.4	1.59	0.43	378
2.04610	5–414	1.3	1.20	0.48	937
2.32180	5–472	1.2	0.92	0.53	1160
3.11460	5–667	1.0	0.65	0.60	1735
3.90050	5–1261	0.6	0.35	0.65	2920
4.39670	5–1559	0.4	0.20	0.70	4488

In the present channel simulations, we report the streamwise spectra $E_{uu}(k_x)$, $E_{vv}(k_x)$, and $E_{ww}(k_x)$ at a near-wall plane and at the channel center in Fig. 4. These spectra are used as scale-by-scale diagnostics of the resolved turbulent motions in the streamwise direction, consistent with established channel-flow DNS studies [29].

5. VALIDATION AGAINST EXPERIMENTS FOR PIPE FLOW

To validate the numerical framework, we compare our pipe-flow simulations against the laser doppler velocimetry (LDV) measurements reported by Guzel et al. [20] for 0.1% Carbopol solutions in a circular pipe. The experimental dataset spans laminar, transitional, and turbulent regimes, which makes it well suited for checking whether the present solver, rheology implementation, and numerical resolution reproduce the observed onset and development of turbulence in a yield-stress, shear-thinning fluid.

In our validation cases, we match the Herschel–Bulkley parameters (τ_y, k, n) and consider the same bulk-velocity range as the experiments. Table 1 summarizes the operating conditions and rheological parameters used for comparison.

The validation focuses on comparisons that are directly accessible in both experiments and simulations. Specifically, we compare (i) the streamwise velocity profile in wall units and in outer scaling, (ii) turbulence intensity trends with increasing Re_G , and (iii) qualitative changes in profile shape associated with the breakdown of the plug-like core as the flow transitions. Agreement across these metrics provides confidence that the present numerical setup reproduces the experimentally observed regime progression and the associated changes in near-wall and core-

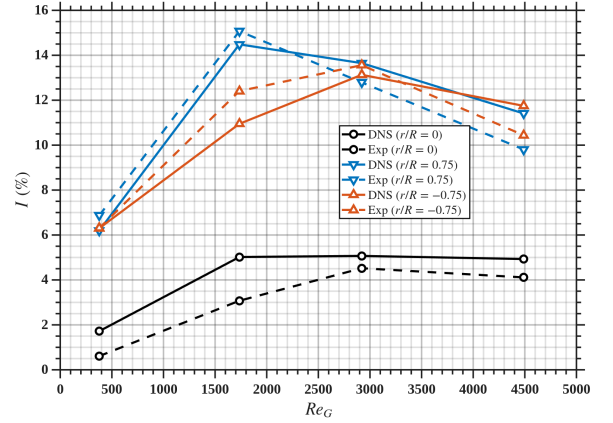


FIGURE 5: Turbulence intensity I (%) as a function of generalized Reynolds number Re_G in Herschel–Bulkley pipe flow. Solid lines with markers show the present DNS, and dashed lines show the experimental data. Results are reported at $r/R = 0$, $r/R = 0.75$, and $r/R = -0.75$.

region dynamics for Herschel–Bulkley pipe flow [20].

5.1. Validation using turbulence intensity trends

To validate the numerical framework against experiments, we compare the radial variation of turbulence intensity as a function of the generalized Reynolds number, using the 0.1% Carbopol pipe-flow measurements of Guzel et al. [20]. Turbulence intensity is used here as a compact measure of the strength of velocity fluctuations relative to the mean flow. At a given radial location, we define

$$I(r) = 100 \frac{u'_{rms}(r)}{U_b}, \quad (20)$$

where $u'_{rms}(r)$ is the root-mean-square of the streamwise velocity fluctuations at radius r , and U_b is the bulk (cross-section averaged) velocity. This definition is consistent with the experimental reporting of turbulence intensity trends and enables a direct comparison between DNS and LDV data.

Figure 5 shows the measured and computed turbulence intensity at three locations, $r/R = 0$ and $r/R = \pm 0.75$. At the lowest Reynolds number considered ($Re_G \approx 378$), the flow is weakly disturbed and remains largely plug-dominated. Yield-stress effects suppress deformation in the core and reduce velocity fluctuations, leading to low turbulence intensity at the centerline. The near-wall locations already exhibit larger values than the centerline because the highest shear occurs in the wall region, where the material is more likely to be yielded and susceptible to unsteady motions.

As Re_G increases into the transitional regime ($Re_G \approx 1735$ to 2920), inertial effects become strong enough to overcome the yield-stress constraint over a larger portion of the cross-section. This promotes the growth of localized instabilities, strengthens near-wall streak-like motions, and accelerates the breakdown of the plug boundary. As a result, turbulence intensity rises sharply, with the strongest fluctuations occurring away from the centerline at $r/R = \pm 0.75$. Both the experiments and the simulations display this behaviour, including the non-monotonic character of the off-center intensity across the transitional window.

At higher Reynolds number ($Re_G \approx 4488$), the flow becomes more broadly turbulent and the intensity decreases slightly at $r/R = \pm 0.75$ compared with its transitional peak. This reduction can occur because the mean flow increases with Re_G while the relative fluctuation level does not grow proportionally, and because the plug resistance becomes less dominant as yielding extends further into the core. Overall, the close agreement between DNS and experiment in terms of (i) the strong radial dependence, (ii) the sharp rise through transition, and (iii) the peak-and-decline trend at the off-center locations supports the fidelity of the present numerical setup for Herschel–Bulkley pipe flow. A small asymmetry is also observed in the turbulence intensity trends. The $I-Re_G$ curves at $r/R = \pm 0.75$ do not coincide perfectly, particularly through the transitional range, consistent with prior experimental reports of asymmetric or biased states in transitional yield-stress and shear-thinning pipe flows (e.g., [18, 20]).

5.2. Vortical structures via Q-criterion

To visualize coherent vortical motions in three-dimensional pipe flow, we use the Q-criterion, which identifies regions where local rotation dominates over strain [12]. For an incompressible flow, Q is defined from the velocity-gradient tensor $\nabla \mathbf{u}$ as

$$Q = \frac{1}{2} \left(\|\boldsymbol{\Omega}\|^2 - \|\mathbf{S}\|^2 \right), \quad (21)$$

where $\mathbf{S} = \frac{1}{2} (\nabla \mathbf{u} + (\nabla \mathbf{u})^T)$ is the strain-rate tensor and $\boldsymbol{\Omega} = \frac{1}{2} (\nabla \mathbf{u} - (\nabla \mathbf{u})^T)$ is the rotation-rate tensor. Positive values of Q indicate rotation-dominated regions, and iso-surfaces of Q provide a convenient way to highlight vortical structures in transitional and turbulent flow fields.

Figures 6 and 7 show representative Q -criterion iso-surfaces for two cases, $Re_G = 4488$ and $Re_G = 378$, together with the corresponding velocity-magnitude legends. At $Re_G = 4488$, the iso-surfaces reveal abundant small-scale vortical activity throughout the pipe, consistent with a fully developed turbulent state. In contrast, at $Re_G = 378$ the flow exhibits comparatively sparse vortical content, with structures that are larger and more organized. This behavior is consistent with a laminar or weakly disturbed regime in which coherent vortical motion is largely confined to the sheared region near the wall, while the core remains weakly sheared due to yield-stress effects.

Overall, the Q-criterion visualizations provide a qualitative view of how coherent flow structures evolve across regimes in Herschel–Bulkley pipe flow, complementing the statistical measures used to classify laminar, transitional, and turbulent behavior.

6. CHANNEL FLOW

Table 2 summarizes the operating conditions and nondimensional groups for the rectangular channel simulations of the 0.1% Carbopol solution modeled as a Herschel–Bulkley fluid. Each case is defined by the imposed mean pressure gradient $\partial p / \partial x$ and the resulting bulk velocity U . For completeness, we also report the wall-based viscosity μ_w , friction velocity u_τ , and friction Reynolds number Re_τ , along with the Herschel–Bulkley parameters (τ_y, κ, n) and the generalized Reynolds number Re_G used to index the transition progression across cases. Figure 8 shows the

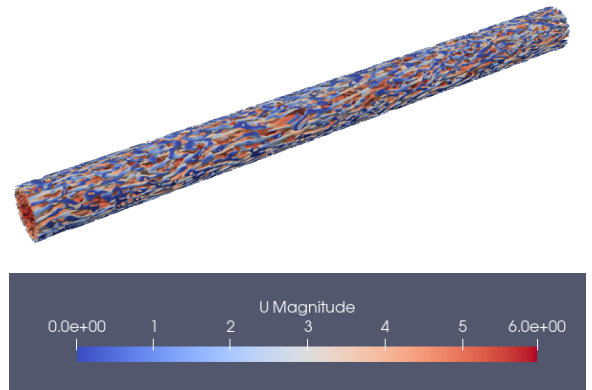


FIGURE 6: Q-criterion iso-surfaces for $Re_G = 4488$ with the corresponding velocity-magnitude legend. The field shows dense small-scale vortical activity consistent with turbulent dynamics.

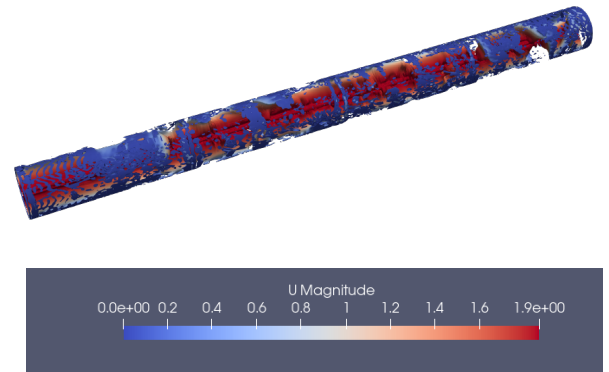


FIGURE 7: Q-criterion iso-surfaces for $Re_G = 378$ with the corresponding velocity-magnitude legend. Vortical structures are comparatively sparse and more coherent, consistent with a laminar or weakly disturbed regime.

normalized, time-averaged streamwise velocity profiles (u/u_c) for the 0.1% Carbopol Herschel–Bulkley channel flow at increasing generalized Reynolds number Re_G . At the lowest Re_G , the profile is strongly blunted, consistent with a plug-dominated core where the shear rate is weak and most of the deformation is confined near the walls. With increasing Re_G , the plug-like region progressively shrinks and the profile becomes fuller across the channel, indicating that a larger fraction of the cross-section participates in the sheared motion. At the highest Re_G , the mean profile approaches the familiar turbulent-channel shape, with a fuller core and steeper near-wall gradients, reflecting the transition from plug-dominated laminar flow to wall-dominated turbulence.

7. CONCLUSION

We performed direct numerical simulations (DNS) of Herschel–Bulkley (HB) yield-stress fluids in both pipe and rectangular channel configurations and resolved the complete progression from laminar flow to fully developed turbulence over a wide range of generalized Reynolds numbers. The simulations capture the yield-stress-driven plug, its gradual erosion with increasing inertia, and the emergence of near-wall turbulent activity

TABLE 2: Channel-flow operating and Herschel–Bulkley parameters for the 0.1% Carbopol cases used in the DNS. The fluid is modeled as Herschel–Bulkley and thixotropic effects are neglected.

U (m/s)	$\partial p/\partial x$ (Pa/m)	μ_w (Pa·s)	u_τ (m/s)	Re_τ	τ_y (Pa)	κ (Pa·s ^{n})	n	Re_G
4.397	11.80	0.01807	0.23646	62.31	0.40	0.20	0.70	1158.69
5.000	12.82	0.01739	0.24709	67.68	0.40	0.20	0.70	1369.51
6.000	29.07	0.01218	0.37208	145.51	0.40	0.20	0.70	2346.45
7.000	35.75	0.01000	0.40000	176.47	0.40	0.20	0.70	2993.59
10.00	58.80	0.008986	0.52918	280.46	0.40	0.20	0.70	5300.00

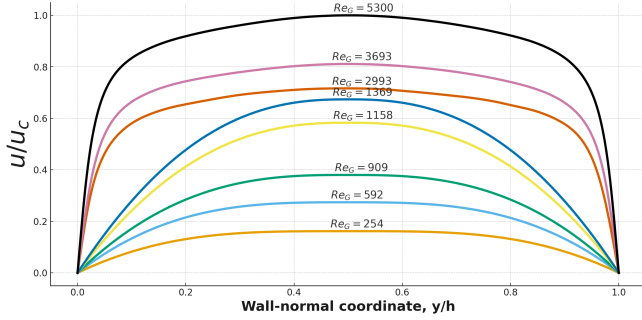


FIGURE 8: Normalized, time-averaged streamwise velocity profiles (u/u_c) in the channel at increasing generalized Reynolds number Re_G for the 0.1% Carbopol Herschel–Bulkley fluid.

during transition.

A key outcome is that transition is controlled by the local competition between turbulent momentum transport and the yield stress: sustained turbulence develops only when Reynolds stresses locally exceed the yield stress, allowing the plug-like core to deform and break down. For pipe flow, the DNS supports a clear regime classification:

- $Re_G < 1735$: laminar regime with a strong plug and negligible turbulence,
- $1735 < Re_G < 2920$: transitional regime with intermittent/decaying turbulence,
- $Re_G > 2920$: fully turbulent regime where the plug breaks down and turbulence becomes established.

The computed turbulence-intensity trends are consistent with available experimental measurements for Carbopol pipe flow reported by Güzel et al. (2009), providing validation of the numerical framework. Finally, the pipe-flow results show evidence of asymmetry in the transitional range, consistent with observations reported in the literature for yield-stress and shear-thinning pipe flows.

ACKNOWLEDGMENTS

This material is based upon work supported by the U.S. Department of Energy’s Office of Energy Efficiency and Renewable Energy (EERE) under the Advanced Manufacturing Office, Award Number DE-EE0009396. Partial financial support was also provided by the Renewable Byproducts Institute Graduate Fellowship. The views expressed herein do not necessarily represent the views of the U.S. Department of Energy or the United

States Government. In disclosure, the part of this work was presented at APS-DFD [31–34].

REFERENCES

- [1] Kumar, Vivek, Jain, Palak, Upadhyay, Ravi Kant, Bharath, KS and Waghmare, Prashant R. “Particle separation using modified Taylor’s flow.” *Microfluidics and Nanofluidics* Vol. 27 No. 10 (2023): p. 66.
- [2] Kumar, Vivek, Quintero, JSM, Baldygin, Aleksey, Molina, Paul, Willers, Thomas and Waghmare, Prashant R. “Viscosity and dynamic surface tension measurement: A guideline for appropriate measurement.” *arXiv preprint arXiv:2510.05481* (2025).
- [3] Kumar, Vivek, Quintero, Jsm, Baldygin, Aleksey, Molina, Paul, Willers, Thomas and Waghmare, Prashant R. “Viscosity and dynamic surface tension measurement: A guideline for appropriate measurement.” *Journal of Colloid and Interface Science* (2026): p. 139929.
- [4] Baldygin, Aleksey, Kumar, Vivek, Willers, Thomas and Waghmare, Prashant. “The effect of viscosity on the relaxation time for surface tension measurement.” *Bulletin of the American Physical Society* Vol. 67 (2022).
- [5] Nayak, Chaitanya S, Mohammed, Faizaan, Kumar, Vivek, Prajapati, Shivam and Aidun, Cyrus. “Depth-Aware Machine Learning Framework for Bubble Characterization in Two-Phase Flows.” *arXiv preprint arXiv:2601.21175* (2026).
- [6] Madanan, Umesh and Prajapati, S. “Computational study on jet break-up behavior of a high-density liquid jet entering a quiescent immiscible liquid pool.” (2021).
- [7] Kumar, Vivek, Kabir, Raihanul, Shannon, Zachary, Waghmare, Prashant R and Flynn, Morris R. “Experimental study on R1234yf/R134a mixture (R513a) as R134a replacement in heat pipes.” *Journal of Enhanced Heat Transfer* Vol. 32 No. 4 (2025).
- [8] Kumar, Vivek and Rahman, Muhammad Rizwanur. “On the hydrostatic limit for thin film flow with applications to thermosyphons.” *Applied Thermal Engineering* Vol. 245 (2024): p. 122869.
- [9] Kumar, Vivek, Suchandra, Prasoon, Javadi, Ardalan, Jain, Suhas S and Aidun, Cyrus. “Bubble coalescence dynamics in a high-Reynolds number decaying turbulent flow.” *arXiv preprint arXiv:2509.05888* (2025).
- [10] Javadi, Ardalan, Kumar, Vivek and Aidun, Cyrus K. “Large eddy simulations of side channel pump in different operating

- conditions.” *Engineering Applications of Computational Fluid Mechanics* Vol. 20 No. 1 (2026): p. 2587723.
- [11] Yusufi, B. K., Kapelan, Z. and Mehta, D. “Advances in modeling the flow of Herschel–Bulkley fluids in pipes: A review.” *Physics of Fluids* Vol. 37 No. 2 (2025): p. 021302. DOI [10.1063/5.0252248](https://doi.org/10.1063/5.0252248).
- [12] Pope, Stephen B. *Turbulent Flows*. Cambridge University Press (2000).
- [13] Wang, Zhongrong, Guo, Wenjing, Ding, Wantao, Liu, Keqi, Qin, Wang, Wang, Chengzhen and Wang, Zhicheng. “Numerical study on the hydrodynamic properties of bentonite slurries with Herschel–Bulkley–Papanastasiou rheology model.” *Powder Technology* Vol. 419 (2023): p. 118375. DOI [10.1016/j.powtec.2023.118375](https://doi.org/10.1016/j.powtec.2023.118375).
- [14] Yusufi, B. K., Kapelan, Z. and Mehta, D. “Rheology-based wall function approach for wall-bounded turbulent flows of Herschel–Bulkley fluids.” *Physics of Fluids* Vol. 36 No. 2 (2024): p. 023112. DOI [10.1063/5.0180663](https://doi.org/10.1063/5.0180663).
- [15] Nishi, M., Unsal, B., Durst, F. and Biswas, G. “Laminar-to-turbulent transition of pipe flows through puffs and slugs.” *Journal of Fluid Mechanics* Vol. 614 (2008): pp. 425–446. DOI [10.1017/S0022112008003504](https://doi.org/10.1017/S0022112008003504).
- [16] Draad, A. A., Kuiken, G. D. C. and Nieuwstadt, F. T. M. “Laminar–turbulent transition in pipe flow for Newtonian and non-Newtonian fluids.” *Journal of Fluid Mechanics* Vol. 377 (1998): pp. 267–312.
- [17] Escudier, M. P., Presti, F. and Smith, S. “Laminar, transitional and turbulent flow of a shear-thinning liquid in a pipe.” *Journal of Non-Newtonian Fluid Mechanics* Vol. 127 No. 2 (2005): pp. 143–155. DOI [10.1016/j.jnnfm.2005.02.010](https://doi.org/10.1016/j.jnnfm.2005.02.010).
- [18] Peixinho, J., Nouar, C., Desaubry, C. and Théron, B. “Laminar, transitional and turbulent flow of yield stress fluids in a pipe.” *Journal of Non-Newtonian Fluid Mechanics* Vol. 128 (2005): pp. 172–184. DOI [10.1016/j.jnnfm.2005.03.008](https://doi.org/10.1016/j.jnnfm.2005.03.008).
- [19] Esmael, A., Nouar, C., Desaubry, C. and Théron, B. “Observations of asymmetrical flow behaviour in transitional pipe flow of yield-stress and other shear-thinning liquids.” *Journal of Non-Newtonian Fluid Mechanics* Vol. 150 No. 1 (2008): pp. 55–67. DOI [10.1016/j.jnnfm.2007.12.010](https://doi.org/10.1016/j.jnnfm.2007.12.010).
- [20] Güzel, B., Burghilea, T., Frigaard, I. and Martinez, D. M. “Observation of laminar–turbulent transition of a yield stress fluid in Hagen–Poiseuille flow.” *Journal of Fluid Mechanics* Vol. 627 (2009): pp. 97–129. DOI [10.1017/S0022112009005813](https://doi.org/10.1017/S0022112009005813).
- [21] Güzel, B., Burghilea, T., Martinez, D. M. and Frigaard, I. A. “Intermittency in the transition to turbulence for a shear-thinning fluid in Hagen–Poiseuille flow.” *Chemical Engineering Science* Vol. 64 No. 14 (2009): pp. 3341–3352. DOI [10.1016/j.ces.2009.03.035](https://doi.org/10.1016/j.ces.2009.03.035).
- [22] Bahrani, S. A., Nouar, C., Sauret, A. and Castelain, C. “Intermittency in the transition to turbulence for a shear-thinning fluid in Hagen–Poiseuille flow.” *Journal of Non-Newtonian Fluid Mechanics* Vol. 214 (2014): pp. 39–51. DOI [10.1016/j.jnnfm.2014.08.002](https://doi.org/10.1016/j.jnnfm.2014.08.002).
- [23] Charles, B., Selin, J., Laudat, A., Vateville, J. and Gillissen, J. J. J. “Asymmetry and intermittency in the rheo-inertial transition to turbulence in pipe flow.” *Physical Review Fluids* Vol. 9 No. 11 (2024): p. 114601. DOI [10.1103/PhysRevFluids.9.114601](https://doi.org/10.1103/PhysRevFluids.9.114601).
- [24] Nikbakht, A., Rad, S. Z., Lundell, F., Östlund, S. and Öiseth, O. “Fibre suspensions in Hagen–Poiseuille flow: Transition from laminar plug flow to turbulence.” *Journal of Non-Newtonian Fluid Mechanics* Vol. 211 (2014): pp. 1–10. DOI [10.1016/j.jnnfm.2014.06.002](https://doi.org/10.1016/j.jnnfm.2014.06.002).
- [25] Erge, O., Babadagli, T. and Javadpour, F. “Laminar to turbulent transition of yield power law fluids in annuli.” *Journal of Petroleum Science and Engineering* Vol. 135 (2015): pp. 185–206. DOI [10.1016/j.petrol.2015.08.026](https://doi.org/10.1016/j.petrol.2015.08.026).
- [26] Metzner, A. B. and Reed, J. C. “Flow of non-Newtonian fluids—correlation of the laminar, transition, and turbulent-flow regions.” *AIChE Journal* Vol. 1 No. 4 (1955): pp. 434–440.
- [27] Rudman, M., Blackburn, H. M., Graham, L. J. W. and Pullum, L. “Turbulent pipe flow of shear-thinning fluids.” *Journal of Non-Newtonian Fluid Mechanics* Vol. 118 No. 1 (2004): pp. 33–48. DOI [10.1016/j.jnnfm.2004.02.006](https://doi.org/10.1016/j.jnnfm.2004.02.006).
- [28] Singh, J., Rudman, M. and Blackburn, H. M. “The influence of shear-dependent rheology on turbulent pipe flow.” *Journal of Fluid Mechanics* Vol. 822 (2017): pp. 848–879. DOI [10.1017/jfm.2017.296](https://doi.org/10.1017/jfm.2017.296).
- [29] Kim, J., Moin, P. and Moser, R. “Turbulence statistics in fully developed channel flow at low Reynolds number.” *Journal of Fluid Mechanics* Vol. 177 (1987): pp. 133–166. DOI [10.1017/S0022112087000892](https://doi.org/10.1017/S0022112087000892).
- [30] Karahan, Dogukan T, Ranjan, Devesh and Aidun, Cyrus K. “Turbulent channel flow of generalized Newtonian fluids at $Re\tau = 180$.” *Journal of Non-Newtonian Fluid Mechanics* Vol. 314 (2023): p. 105015.
- [31] Prajapati, Shivam, Suchandra, Prasoon, Kumar, Vivek, Javadi, Ardanan and Aidun, Cyrus K. “Laminar–Turbulent Transition in Yield-Stress Fluids in Channel and Pipe Flow: Experimental and DNS Study.” *Division of Fluid Dynamics Annual Meeting 2025*. 2025. APS.
- [32] Suchandra, Prasoon, Kumar, Vivek, Rom, Jason, Prajapati, Shivam, Javadi, Ardanan, Jain, Suhas S and Aidun, Cyrus K. “Surfactant-induced suppression of bubble coalescence in turbulent duct flow at high Reynolds numbers.” *Division of Fluid Dynamics Annual Meeting 2025*. 2025. APS.
- [33] Kumar, Vivek, Suchandra, Prasoon, Prajapati, Shivam, Javadi, Ardanan, Jain, Suhas S and Aidun, Cyrus K. “Bubble-Mass Cascade in Decaying Turbulent Flows.” *Division of Fluid Dynamics Annual Meeting 2025*. 2025. APS.
- [34] Kumar, Vivek, Javadi, Ardanan, Jain, Suhas and Aidun, Cyrus. “On the coalescence of bubbles in highly turbulent flows.” *Bulletin of the American Physical Society* (2024).